Earth and Planetary Science Letters 591 (2022) 117620

Contents lists available at ScienceDirect

Earth and Planetary Science Letters

www.elsevier.com/locate/epsl

Homogenising the upper continental crust: The Si isotope evolution of the crust recorded by ancient glacial diamictites

Madeleine E. Murphy [a,*], Paul S. Savage [a], Nicholas J. Gardiner [a], Anthony R. Prave [a], Richard M. Gaschnig [b], Roberta L. Rudnick [c]

[a] School of Earth and Environmental Sciences, University of St Andrews, Bute Building, Queen's Terrace, St Andrews, KY16 9TS, Scotland, United Kingdom
[b] Department of Environmental, Earth and Atmospheric Sciences, University of Massachusetts Lowell, Lowell, MA 01854, United States
[c] Department of Earth Science, University of California, Santa Barbara, CA 93106, United States

ARTICLE INFO

Article history:
Received 30 January 2022
Received in revised form 11 May 2022
Accepted 14 May 2022
Available online xxxx
Editor: L. Coogan

Keywords:
silicon isotopes
upper continental crust
glacial diamictites
crustal reworking
secular change

ABSTRACT

Twenty-four composite samples of the fine-grained matrix of glacial diamictites deposited from the Mesoarchaean to Palaeozoic have been analysed for their silicon isotope composition and used to establish, for the first time, the long-term secular Si isotope record of the compositional evolution of upper continental crust (UCC). Diamictites with Archaean and Palaeoproterozoic Nd model ages show greater silicon isotope heterogeneity than those with younger model ages (irrespective of depositional age). We attribute the anomalously light Si isotope compositions of some diamictites with Archaean model ages to the presence of glacially milled banded iron formation (BIF), substantiated by the high iron content and Ge/Si in these samples. We infer that relatively heavy Si isotope signatures in some Palaeoproterozoic diamictites (all of which have Archaean Nd model ages) are due to contribution from tonalite-trondhjemite-granodiorites (TTGs), evidenced by the abundance of TTG clasts. By the Neoproterozoic (with model ages ranging from 2.3 to 1.8 Ga), diamictite Si isotope compositions exhibit a range comparable to modern UCC. This reduced variability through time is interpreted as reflecting the decreasing importance of BIF and TTG in post-Archaean continental crust. The secular evolution of Si isotopes in the diamictites offers an independent test of models for the emergence of stable cratons and the onset of horizontal mobile-lid tectonism. The early Archaean UCC was heterogeneous and incorporated significant amounts of isotopically light BIF, but following the late Archaean stabilisation of cratons, coupled with the oxygenation of the atmosphere that led to the reduced neoformation of BIF and diminishing quantities of TTGs, the UCC became increasingly homogeneous. This homogenisation likely occurred via reworking of preexisting crust, as evidenced by Archaean Nd model ages recorded in younger diamictites.

1. Introduction

The evolution of continental crust is crucially linked to the differentiation of our planet (e.g. Jacobsen et al., 2008; Halliday, 2014), the establishment of plate tectonics (e.g. Brown et al., 2020; Hawkesworth et al., 2020; Tang et al., 2016), and the rise of atmospheric oxygen (e.g. Canfield, 2014; Lee et al., 2016). A key archive for investigating this evolutionary trajectory is the chemical composition of sedimentary rocks, of which glacial diamictites are an important example. Diamictites are an established proxy for ascertaining the average composition of upper continental crust (UCC) exposed at Earth's surface during glaciation (Gaschnig et al., 2014). Four glacial intervals are observed between ~2.9 and 0.3 Ga from diamictites deposited by continental ice sheets on several modern continents. These diamictites are used as tracers of secular changes in UCC composition, and as archives for interrogating climatic and tectonic phenomena such as the shift in weathering style due to atmospheric oxygenation (Gaschnig et al., 2014; Li et al., 2016; S.-J. Wang et al., 2019; Greaney et al., 2020), the relative heterogeneity of Archaean upper mantle (Mundl et al., 2018) and the evolution of bulk continental crust composition (and formation processes) from the Hadean to the Phanerozoic (Gaschnig et al., 2014, 2016; Tang et al., 2016; Chen et al., 2020). Further, diamictite samples have yielded insights into temporal changes in UCC siderophile, chalcophile, and platinum group element concentrations (Chen et al., 2016, 2020; Gaschnig et al., 2014, 2016).

As silicon is the second most abundant element in the continental crust (Rudnick and Gao, 2014), Si isotope geochemistry is a

* Corresponding author.
E-mail address: mm439@st-andrews.ac.uk (M.E. Murphy).

https://doi.org/10.1016/j.epsl.2022.117620

natural tool for evaluating crustal evolution. This system is resistant to metamorphism (Savage et al., 2013a; B. Wang et al., 2019), but sensitive to igneous differentiation (Savage et al., 2012, 2014) and weathering reactions, such as clay neoformation (e.g. Opfergelt et al., 2012; Ziegler et al., 2005), making it useful for understanding both high- and low-temperature processes recorded in the rock record. Because silicon in the crust is dominantly derived from the mantle, the stable Si isotope composition of the bulk silicate Earth (BSE) can be used as a metric against which to measure other silica reservoirs (Savage et al., 2014). Silicon isotope signatures of the BSE, modern UCC, and Phanerozoic loess and shales can be used as baselines for understanding processes like igneous differentiation and chemical weathering in older crustal material to elucidate secular changes in the upper continental crust.

Here we utilise, for the first time, stable silicon isotopes to study ancient diamictites. We report the silicon isotope composition of 24 diamictite composites across four ancient glacial periods to establish a baseline global Si isotope record for the UCC from the Archaean to Palaeozoic. In addition, we assess the response of the silicon isotope system to known secular and regional changes inherent to particular cratons, such as the presence of banded-iron formation (BIF).

2. Silicon isotopes

Silicon has three stable isotopes, from most to least abundant: ^{28}Si, ^{29}Si and ^{30}Si. Silicon isotope compositions are quoted in delta notation, δ^{30}Si or δ^{29}Si, as the permil (‰) deviation from the NBS28 standard:

$$\delta^{X}\mathrm{Si} = [(^{X}\mathrm{Si}/^{28}\mathrm{Si}_{\mathrm{sample}}/^{X}\mathrm{Si}/^{28}\mathrm{Si}_{\mathrm{NBS28}}) - 1] \times 1000$$

where $x = 29$ or 30. The δ^{30}Si composition of the BSE, -0.29 ± 0.07‰ (2 s.d., Savage et al., 2014), and average UCC, -0.25 ± 0.16‰ (2 s.d., Savage et al., 2013b), are used as benchmarks for δ^{30}Si data in crustal material. Resolvable silicon isotope fractionation can result from both high- and low-temperature processes. For example, Si isotope values in igneous rocks usually define a relatively narrow range (~0.30‰; Poitrasson, 2017 and references therein) which correlates positively with degree of igneous differentiation. Conversely, material derived from low-temperature processes displays larger ranges in δ^{30}Si, such as the 0.82‰ range of modern shales (Savage et al., 2013b), and larger range of ~2.5‰ in soils (Poitrasson, 2017 and references therein). Surface processes can impart significant mass-dependent Si isotope fractionations (e.g. Georg et al., 2009); neoformation of clay minerals will drive δ^{30}Si to relatively negative values (Opfergelt et al., 2012; Ziegler et al., 2005), down to an average -2.2‰ in secondary kaolinites in granitic saprolite (Ziegler et al., 2005). Adsorption of silica onto iron oxyhydroxides (e.g. Delstanche et al., 2009) drives δ^{30}Si to negative values, exemplified by very low δ^{30}Si signatures from banded iron formations (BIF; Chakrabarti et al., 2012; Delvigne et al., 2012), down to -4.29‰ (Chakrabarti et al., 2012). Conversely, precipitation of silica from seawater, with a modern-day δ^{30}Si of ~ +1.1‰ (De La Rocha et al., 2000), imparts positive δ^{30}Si in authigenic seawater-derived silica (with respect to the bulk silicate Earth, BSE).

Variations in δ^{30}Si in continental crust over time may record major tectonic and atmospheric changes as crust evolved and began to interact with the hydrosphere. Recent studies of Archaean granitoids (i.e. tonalite-trondhjemite-granodiorites, TTGs) found anomalously high δ^{30}Si compared to modern granites, attributed to incorporation of seawater-derived Si in their source regions caused by specific formation process(es) of TTG melt (André et al., 2019; Deng et al., 2019). As the processes forming modern continental crust are thought to be significantly different from those producing TTGs, the heavy Si signatures of TTGs compared to modern analogues imply there should exist a decreasing average crustal δ^{30}Si over time. Increased oceanic Si delivery from oxidative weathering of crust, combined with the evolution of silica-utilising organisms in the oceans no doubt changed the Si isotope composition of seawater over time, producing marine sediments with variable silicon isotope signatures (Marin-Carbonne et al., 2014).

Consequently, measurement of silicon isotopes in ancient glacial diamictites can potentially elucidate tectono-magmatic and surface processes that shaped the UCC. The robustness of silicon isotopes up to granulite facies metamorphism (Savage et al., 2013a) affords the opportunity to look through multi-generations of orogeny to assess primary signatures of the continental crust through time. Hence, Si isotopes potentially track secular climatic and geologic changes and, applied here to ancient glacial diamictites, may provide an evolving record of the composition of UCC and its response to major coeval geological events.

3. Materials and methods

3.1. Samples

We analysed 24 glacigenic diamictite composites compiled from individual samples from outcrops and drillcores (Table 1, collected and characterised by Gaschnig et al., 2014, 2016) that comprise 100+ individual diamictite samples and span four periods of inferred glaciations in the Mesoarchaean (~2.9 Ga), Palaeoproterozoic (~2.4-2.2 Ga), Neoproterozoic (~0.78-0.52 Ga) and Palaeozoic (~0.3 Ga) (Fig. 1). These same samples have been analysed extensively by other workers who have: (i) shown decreasing Cu concentrations and Cu/Ag ratios at ~3.0-2.4 Ga inferred to mark a transition from basaltic- to felsic-dominated crust (Chen et al., 2020); (ii) demonstrated a shift to lower Mo concentrations and lighter Mo isotopes interpreted to time the Great Oxidation Event and subsequent onset of oxidative weathering (Gaschnig et al., 2014; Greaney et al., 2020); (iii) shown that heterogeneous ^{182}W isotope values typify Archaean diamictites, attributed to the influence of unusual komatiites in Archaean UCC of the Kaapvaal craton (Mundl et al., 2018); (iv) used them to produce an updated average UCC chemical composition through time (Gaschnig et al., 2016). In total, the diverse body of geochemical research focused on these samples documents a robust, multi-proxy record of secular change in the composition of the upper continental crust.

Samples used to form the composites mostly consisted of massive, muddy to sandy diamictite matrices with pebble-sized and larger clasts, with minor dropstone-containing argillites spatially related to the diamictites. Clasts > 5 mm were removed and the resulting fine-grained matrix ground in an alumina jaw crusher. Composites of each stratigraphic unit were generated by completely mixing equal parts by weight of several samples within an individual diamictite unit to form a homogeneous powder (Gaschnig et al., 2016). The composite samples cover a large range in chemical compositions (Table S1), from ~32–76 wt% SiO_2; trends in their major element compositions are dictated mainly by quartz to feldspar/clay ratio, except samples with high carbonate or iron content (Gaschnig et al., 2016; Fig. S1).

3.2. Si isotope sample processing – alkali fusion and column chemistry

Sample powders were analysed at the University of St Andrews Isotope Geochemistry (STAiG) facility following analytical procedures after Savage and Moynier (2013); this alkali fusion method was formulated by Georg et al. (2006). To ensure final solution concentrations of 10–30 ppm Si, ~10 mg of sample was weighed into a clean 99.99% pure Ag crucible. Two ~100 mg pellets of 99.99% NaOH flux (Honeywell, semiconductor grade)

Table 1
Diamictite composite sample locality, age, and notable compositional features.

	Composite sample	Approx. depositional age (Ga)	Latitude*	Longitude*	Drillcore depth	Compositional characteristics
Mesoarchaean						
South Africa	Mozaan	2.97	−27.422	31.275		highest FeO_T, BIF-associated
	Afrikander	2.96	−26.599	28.443		highest MgO; silicified
	Promise	2.96	−26.837	26.510	1235 m	komatiite-associated
	Coronation	2.96	−26.837	26.510	956–999 m	komatiite-associated
Palaeoproterozoic						
South Africa	Duitschland	2.40	−26.471	27.597	1191–1192 m	claystone and carbonate fragments
			−26.435	27.661	647.5–648.5 m	
	Timeball Hill	2.23	−26.471	27.597	574.5–583 m	chert clasts in mudstone matrix
	Makganyene	2.33	−28.852	23.147	25–44 m	high FeO_T, BIF-associated
Ontario, Canada	Ramsay Lake	2.38	46.511	−82.597		granitoid & quartzite clasts
	Bruce	2.38	46.413	−82.670		granitoid & quartzite clasts
	Gowganda	2.38	46.774	−81.608		granitoid & quartzite clasts
Wyoming, USA	Bottle Creek	2.38	41.165	−107.177		schistose feldspathic quartzite
Neoproterozoic						
Newfoundland, Canada	Gaskiers	0.58	46.877	−53.616		varied igneous & sediment clasts
Idaho, USA	Pocatello	0.69	42.781	−112.352		granitoid & quartzite clasts
Virginia, USA	Konnarock	0.67	36.675	−81.609		dominant granitoid clasts
China	Nantuo	0.65	30.551	111.057		varied igneous & sediment clasts
	Gucheng	0.68	30.557	111.056		sandy till, varved clay
Namibia	Blaubeker	0.69	−22.956	18.726		highest SiO_2, granitoid clasts
	Kaigas	0.76	−27.864	16.875		granitoid & arenite clasts
	Chuos	0.69	−18.122	13.884		granitoid & sedimentary clasts
	Numees	0.65	−28.105	16.881		granitoid & carbonate clasts
	Ghaub	0.64	−20.406	14.338		lowest SiO_2, limestone clasts
Palaeozoic						
Bolivia	Bolivia	0.31	–	–		quartz, granite, & arenite clasts
South Africa	Dwyka East	0.30	−28.089	31.045		quartz, feldspar, & granite clasts
	Dwyka West	0.30	−29.130	23.130		relatively high FeO_T, BIF clasts

All sample data are from Gaschnig et al. (2014, 2016). *Latitude and longitude are for representative individual samples, not composites. For detailed locality data on individual diamictite samples and general references for each stratigraphic unit see Gaschnig et al., 2016.

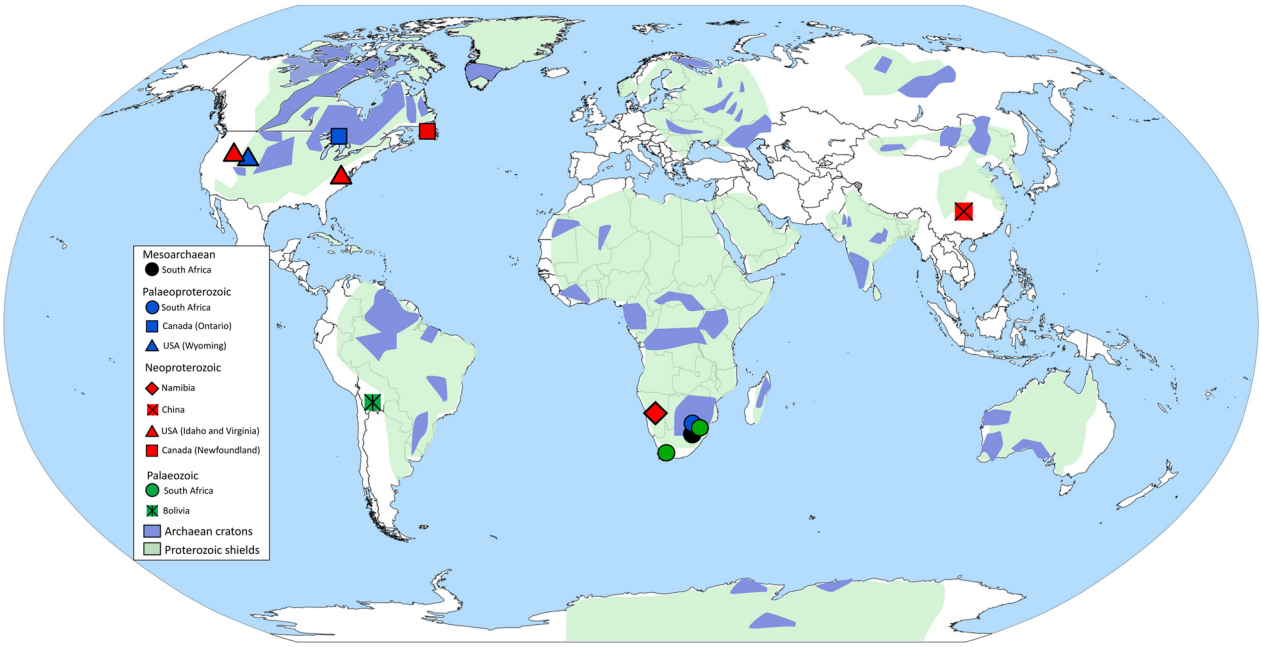

Fig. 1. Distribution of diamictite samples (after Gaschnig et al., 2014) on their respective Archaean cratons and Proterozoic shield areas (after Furnes et al., 2015). (For interpretation of the colours in the figure(s), the reader is referred to the web version of this article.)

were added; NaOH flux recovers >95% of the sample during fusion and only adds Na^+ to the solution, simplifying subsequent ion-chromatography separation. The crucible was then heated in a 720 °C muffle furnace for ~20 min. This crucible, containing fused sample powder, was then cooled and quickly submerged in high purity water of resistivity 18.2 MΩ·cm (deionised with a MilliQ-element, MQ-e, water purifier), to quench and equilibrate overnight in a capped vial. The vial was then agitated at 60 °C by ultrasonic bath so the sample fusion cake could be transferred from the crucible. The crucible was rinsed several times with MQ-e water and all sample was transferred via pipette to solution into a pre-cleaned polypropylene bottle, and then diluted with further deionised water and acidified with HNO_3. To check Si concentration, the Heteropoly Blue methodology was followed, and Si yield was measured using a Thermo Scientific Evolution 60 desktop photospectrometer. The sample was then prepared for analysis using

ion exchange chromatography. A column procedure using cation exchange resin (BioRad AG50 X12, 200-400 mesh) was pursued (after Georg et al., 2006; see also Savage and Moynier, 2013), wherein 1.8 mL of resin is placed into BioRad PolyPrep columns and cleaned (via a procedure in Table S2). After this, sample solutions were loaded onto the columns to yield a final ~2.0 ppm Si in 10 mL of solution (see Table S3 for exact recipe).

3.3. Si isotope mass spectrometry

Isotope measurements were conducted at STAiG on a Neptune Plus Multi Collector Inductively Coupled Plasma Mass Spectrometer (MC-IC-PMS) operating at medium resolution to minimise polyatomic interferences (see Table S4 for operating parameters). Silicon isotope ratios were measured in 25 cycles of ~8-second integrations, reported as averages in Thermo Neptune Data Evaluation software, and blank-corrected to calculate new ratios that we report as δ^{30}Si. The standard NBS28 (now NIST RM8546), a quartz sand, bracketed samples during MC-ICP-MS analyses. The external standards BHVO-2 (basalt, USGS), Diatomite (UCSB), and GSP-2 (granodiorite, USGS) were measured to assess data accuracy and long-term precision. A standard-blank-sample bracketing protocol relative to the NBS28 standard was followed to correct for mass bias and instrumental drift. Measurements were conducted in each session using 12 samples, and each run included NBS28 and external standard BHVO-2; the external standards GSP-2 and Diatomite were also measured several times (Table S5). Samples were analysed in a sequence (bracketed by NBS28) that was repeated three to five times. Silicon isotope compositions (δ^{30}Si values) were calculated using standard-sample bracketing technique; isotope data are reported in terms of δ^{30}Si values and are mass-dependent such that δ^{30}Si values are approximately twice those of δ^{29}Si (Fig. S2), serving as a check of data quality.

4. Results

4.1. External standards

Data accuracy was determined by repeat analysis of external standards BHVO-2, Diatomite, and GSP-2, which are well-characterised for silicon isotopes (see Table S5 for standard data). Reported δ^{30}Si values represent a mean of 3-5 MC-ICP-MS analyses of the same sample solution (denoted by 'n') and our results of $\delta^{30}\text{Si} = 1.24 \pm 0.06$‰ (2 s.d., $n = 5$) for Diatomite, $\delta^{30}\text{Si} = -0.30 \pm 0.04$‰ (2 s.d., $n = 8$) for BHVO-2, and $\delta^{30}\text{Si} = -0.23 \pm 0.06$‰ (2 s.d., $n = 4$) for GSP-2, agree with those in the literature (Table S5). Long-term precision is estimated to be ±0.06‰ (2 s.d.) from repeated measurements of Diatomite and GSP-2.

4.2. Glacial diamictites

All diamictite Si isotope data are given in Table 2. Uncertainties are reported using two standard deviations from the mean (2 s.d.) and standard error at the 95% confidence level (95% s.e.); 95% s.e. $= (t \times s.d.)/\sqrt{n}$, where t is the inverse survival function of the Student's t-test (for the 95% significance level, at $n - 1$ degrees of freedom), and n represents repeated measurements of the same aliquot. Whole-rock δ^{30}Si values for diamictite composites range from −1.17 ± 0.04‰ (95%s.e.) to −0.05 ± 0.05‰ (95% s.e., Fig. 2).

4.2.1. Mesoarchaean diamictites

The Mesoarchaean samples come from the Kaapvaal craton, South Africa, and exhibit the largest range in δ^{30}Si, from −1.17 ± 0.08‰ (2 s.d.) to −0.25 ± 0.05‰ (2 s.d.), and lowest average value of −0.50‰. The anomalously low value of −1.17 ± 0.08‰ for the Mozaan diamictite is a clear outlier (much more negative

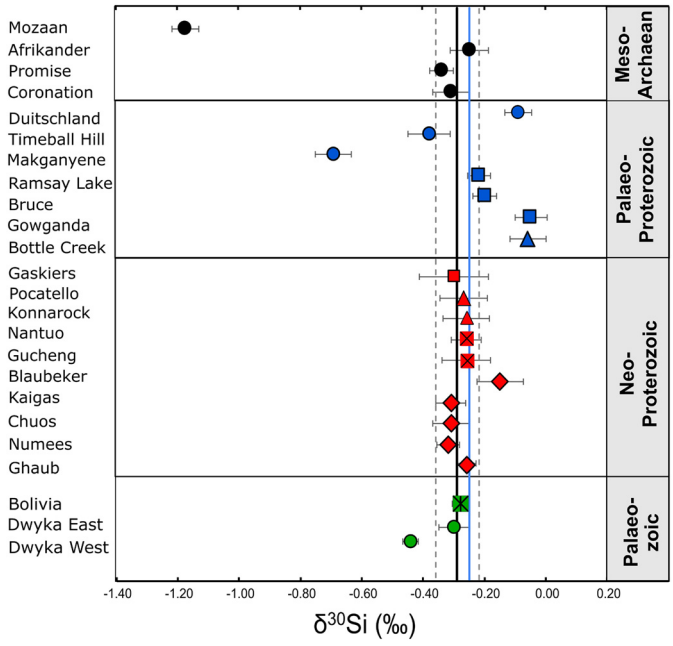

Fig. 2. Plot of δ^{30}Si values for glacial diamictite composite samples. Error bars are two standard deviations (2 s.d.). Blue line is the average modern UCC −0.25‰ δ^{30}Si (Savage et al., 2013b) and black line is −0.29 ± 0.07‰ $\delta^{30}\text{Si}_{\text{BSE}}$ (Savage et al., 2014); dashed lines represent 2 s.d. error on the BSE. Symbols as in Fig. 1.

than δ^{30}Si for average Phanerozoic loess of −0.22 ± 0.07‰ (2 s.d.), from Savage et al., 2013b). The other three Mesoarchaean diamictite composites have values approaching the UCC δ^{30}Si value, −0.25 ± 0.16‰ (2 s.d., Savage et al., 2013b).

4.2.2. Palaeoproterozoic diamictites

Palaeoproterozoic diamictite samples also show a large δ^{30}Si range, from −0.69 ± 0.11‰ (2 s.d.) to −0.05 ± 0.10‰ (2 s.d.), and include the heaviest diamictite composite with δ^{30}Si of −0.05‰ for the Gowganda Formation, Ontario, Canada. Two other diamictites have high δ^{30}Si: Bottle Creek, Wyoming USA, and Duitschland, South Africa, samples with δ^{30}Si of −0.06 ± 0.11‰ (2 s.d.) and −0.09 ± 0.07‰ (2 s.d.), respectively. This group contains a highly negative δ^{30}Si value of −0.69‰ for the South African Makganyene diamictite, illustrating the heterogeneity of Si isotopes in the Palaeoproterozoic.

4.2.3. Neoproterozoic diamictites

Ten diamictite composites cover the Neoproterozoic glacial events across the widest geographic distribution of any of the sample sets (Newfoundland, China, Idaho and Virginia USA, Namibia) yet exhibit a narrow range in δ^{30}Si, from −0.32 ± 0.07‰ (2 s.d.) to −0.15 ± 0.06‰ (2 s.d.). Further, their average of −0.27‰ approximates the Phanerozoic UCC value of −0.25‰. A slightly heavy outlier is the Blaubeker diamictite with a δ^{30}Si value of −0.15‰, but this is within error of the modern UCC value.

4.2.4. Palaeozoic diamictites

Three Palaeozoic composites show a limited range in δ^{30}Si: −0.44 ± 0.05‰ (2 s.d.) for Dwyka West, −0.30 ± 0.09‰ (2 s.d.) for Dwyka East and −0.28 ± 0.02‰ (2 s.d.) for the Bolivia composite.

Whereas the Dwyka East and Bolivia samples approach the modern UCC δ^{30}Si value, Dwyka West is slightly negative, falling outside the 2 s.d. modern UCC error range. Notably, Dwyka West, deposited on the Kaapvaal craton, has an Archaean Nd model age (Mundl et al., 2018; Gaschnig et al., 2022), contains Palaeoproterozoic and Archaean zircons (Gaschnig et al., 2022), and shows

Table 2
Si isotope data for glacial diamictite composite samples.

Composite	Age range (Ma)[1]	~T_{DM} (Ma)[2]	Location	SiO_2 (wt%)	$\delta^{30}Si$ (‰)	2s.d.	95%s.e.	$\delta^{29}Si$ (‰)	2s.d.	95%s.e.	*n*
Mozaan	2980-2954	3320	S Africa	57.20	−1.17	0.08	0.04	−0.60	0.09	0.05	6
Afrikander	2981-2935	3340	S Africa	63.30	−0.25	0.05	0.06	−0.12	0.04	0.05	3
Promise	2981-2935	3380	S Africa	70.30	−0.34	0.04	0.02	−0.16	0.04	0.02	3
Coronation	2981-2935	3290	S Africa	72.00	−0.31	0.06	0.04	−0.14	0.05	0.03	5
Duitschland	2480-2310	2910	S Africa	55.10	−0.09	0.07	0.04	−0.03	0.07	0.04	5
Timeball Hill	2256-2193	2895	S Africa	65.00	−0.38	0.07	0.04	−0.21	0.09	0.06	3
Makganyene	2431-2222	2895	S Africa	56.70	−0.69	0.11	0.06	−0.37	0.04	0.02	6
Ramsay Lake	2450-2308	2900	Ontario	67.90	−0.22	0.07	0.04	−0.09	0.06	0.03	6
Bruce	2450-2308	3010	Ontario	67.90	−0.20	0.03	0.04	−0.08	0.07	0.09	3
Gowganda	2450-2308	2940	Ontario	65.80	−0.05	0.10	0.05	−0.01	0.05	0.03	6
Bottle Creek	2460-2090	3030	Wyoming	71.00	−0.06	0.11	0.06	−0.03	0.08	0.04	6
Gaskiers	581-580	1093	Newfoundland	66.80	−0.30	0.09	0.11	−0.16	0.04	0.05	3
Pocatello	705-667	-	Idaho	69.30	−0.27	0.08	0.05	−0.18	0.09	0.06	5
Konnarock	760-570	-	Virginia	67.50	−0.26	0.06	0.07	−0.12	0.1	0.12	3
Nantuo	655-635	-	China	65.10	−0.26	0.04	0.05	−0.10	0.12	0.15	3
Gucheng	703-655	-	China	66.50	−0.26	0.08	0.05	−0.15	0.04	0.02	5
Blaubeker	746-635	2040	Namibia	76.80	−0.15	0.06	0.07	−0.06	0.05	0.06	5
Kaigas	771-741	2310	Namibia	63.80	−0.31	0.05	0.03	−0.18	0.09	0.06	5
Chuos	746-635	2000	Namibia	47.10	−0.31	0.06	0.04	−0.15	0.03	0.02	5
Numees	741-555	1780	Namibia	70.70	−0.32	0.07	0.04	−0.15	0.04	0.02	6
Ghaub	637-633	1840	Namibia	32.00	−0.26	0.06	0.03	−0.14	0.04	0.02	6
Bolivia	326-299	1751	Bolivia	73.60	−0.28	0.02	0.02	−0.13	0.06	0.07	3
Dwyka East	312-288	1910	S Africa	67.30	−0.30	0.09	0.05	−0.15	0.06	0.03	6
Dwyka West	312-288	2545	S Africa	42.80	−0.44	0.05	0.03	−0.21	0.07	0.04	6

[1]Age range from Gaschnig et al. (2014). [2]Nd model ages (T_{DM}) from Gaschnig et al. (2022).

transition metal enrichments comparable to Mesoarchaean samples (Gaschnig et al., 2016).

5. Discussion

Silicon isotope data for glacial diamictite composites show a broad secular trend: those deposited before ~2.5 Ga have relatively heterogeneous Si isotope values ($\delta^{30}Si = -1.17‰$ to $-0.05‰$), whereas by the Neoproterozoic this range is significantly reduced to an average value indistinguishable from modern UCC. Here we address potential sources of diamictite Si isotope heterogeneity and consider how the temporal $\delta^{30}Si$ trends and associated geochemical data may reflect global tectonic phenomena and geodynamic change.

5.1. Linking diamictites to the evolution of continental crust

Glacial diamictites have been established as robust representatives of UCC because they provide averages of physically eroded, widespread bedrock, and- barring the limited geographic extent of the Mesoarchaean samples- their extensive provenance and widespread geographic distribution within the same time intervals (e.g. Palaeozoic and Neoproterozoic) make them useful for tracking secular changes in global UCC (Gaschnig et al., 2014). These 24 glacial diamictite composites have been interpreted as useful proxies of the average UCC chemical composition (e.g. Chen et al., 2020; Gaschnig et al., 2014, 2016; Greaney et al., 2020; Li et al., 2016; Mundl et al., 2018; Tang et al., 2016; S.-J. Wang et al., 2019). Because these samples reflect chemical changes in the crust over time, the diamictite Si isotope data herein are interpreted to record the secular evolution of the $\delta^{30}Si$ composition of the UCC.

In interpreting silicon isotope data from ancient rocks, the question arises whether such data reflect original compositions of the rocks, or whether they record a degree of secondary alteration. Given that glacial diamictites are derived from physical weathering under cold climates, $\delta^{30}Si$ compositions would have been minimally influenced by temperature-related chemical alteration or fractionation during glaciation. Additionally, these diamictites were largely deposited in marginal marine environments and buried rapidly, evidenced by overlying conformable sediments (as discussed in Li et al., 2016), supporting the idea that the diamictites preserve original $\delta^{30}Si$ signatures of the upper crust they eroded. The lack of weathering horizon indicators in the diamictite stratigraphy combined with their Pb isotope systematics suggest the weathering signature of these diamictites is inherited from the UCC over which the glaciers flowed (Li et al., 2016). Furthermore, because whole-rock Si isotope compositions are resistant to metamorphism up to granulite facies (Savage et al., 2013a), metamorphic processes have likely had little impact on the original Si isotope signatures. Hence, we are confident that the $\delta^{30}Si$ values are not recording signatures generated via post-depositional secondary alteration or metamorphism, and their signatures accurately reflect that of the source material sampled, i.e., the ancient continental crust. Thus, their heterogeneous nature reflects original crustal heterogeneity.

5.2. Sources of Si isotope heterogeneity in the ancient upper continental crust

The South African Mozaan and Makganyene diamictites stand out due to their highly negative $\delta^{30}Si$ values. One explanation is presence of clay-rich material in their protoliths, a reasonable inference given that Mozaan Group shales show values down to $-0.86‰$ (Delvigne et al., 2016). Because diamictite $\delta^{30}Si$ values record the composition of rocks sampled by glaciers, they may indicate the degree of weathering the ancient continental crust experienced prior to glaciation. This process is, however, complicated by the variably weathered mixture of regolith and bedrock comprising each diamictite composite, which should have an averaging effect on source lithologies with distinct isotopic values (Greaney et al., 2020). If highly negative Si isotope signatures are a result of clay mineral formation in diamictite protoliths, there would have to be enough clay minerals present in the majority of diamictites included in the composites to drive the overall signature to negative values; this should therefore be reflected in a mineralogical or compositional indicator of high clay abundance. However, the *low*

Al_2O_3 content of the most negative diamictite samples (Mozaan at 8.70 wt% and Makganyene at 8.30 wt%) compared to the other diamictites (and the average UCC of 15.40 wt%; Rudnick and Gao, 2014) indicates that incorporation of clay minerals from source rocks is not the main cause of the low δ^{30}Si signature. This conclusion is supported by the fact that the SiO_2 and Al_2O_3 contents of the Mozaan and Makganyene samples cannot be explained as binary clay/feldspar mixtures (Fig. S1), as these are more influenced by Fe-dilution than the other diamictites (Gaschnig et al., 2016). Additionally, if clays were the source of the light Si signatures there should be a correlation between δ^{30}Si and chemical index of alteration (CIA) values, which is not observed in the composites (Fig. S3). Chemical weathering-derived, clay-rich material in the source can therefore be ruled out as a cause of the anomalously light Si isotope compositions in these composite samples (for a discussion of how Archaean weathering may impact these interpretations, see Appendix A).

Another process that generates negative Si isotope values is formation of glacially-derived silicon. Dissolvable amorphous silica (ASi) is a subglacial weathering product representing a major downstream Si flux in glacial environments; values of $\delta^{30}Si_{ASi}$ down to −0.86‰ were reported in meltwaters from sub-Arctic glaciers (Hatton et al., 2019). However, driving whole-rock Si isotope values to such extreme negative values necessitates substantial amounts of glacial ASi, requiring that diamictites originally containing high ASi be quite SiO_2-rich. Of the samples, Mozaan and Makganyene are mid-range for their silica content, at 57.20 and 56.70 wt%, respectively (Fig. S4), thus glacial ASi is an unlikely source for the isotopically light signatures. Both Mozaan and Makganyene are polymict (containing clasts of various lithologies) and, although both diamictite units are known to contain chert clasts (see references within Gaschnig et al., 2014), there would have to be a significant ASi fraction in the matrix, which is not supported by their SiO_2 composition. Moreover, if ASi was significant in controlling δ^{30}Si, then all glaciogenic diamictite samples should have light Si compositions relative to UCC (or at least in the most siliceous samples). However, this is not observed, and the most silica-rich sample, Blaubeker, has a slightly high δ^{30}Si signature (−0.15‰). Additionally, although the −0.69‰ δ^{30}Si value for the Makganyene diamictite is less negative than the lowest $\delta^{30}Si_{ASi}$ value for glacial meltwater, the Mozaan value at −1.17‰ is far below the known ASi range. In rock crushing experiments mimicking subglacial processes, the $\delta^{30}Si_{ASi}$ average is −0.22 ± 0.15‰ (2 s.d, Hatton et al., 2021). Therefore, ASi is unlikely to be a significant source of the anomalous diamictite Si signatures.

The most likely explanation for the low δ^{30}Si values of the Mozaan and Makganyene diamictites (and the slightly low δ^{30}Si Dwyka West composite) is a major iron formation component in their provenance. The Mozaan δ^{30}Si composition is the most negative of our data, and more negative than that of younger deposits like shales. Such strong negative Si isotope fractionation is found only in highly weathered material or BIF, from adsorption of silica onto iron oxyhydroxides (Delstanche et al., 2009). The Mozaan δ^{30}Si value is therefore likely a result of the presence of BIF in the diamictite provenance, as the Pongola BIF is one of its predominant associated lithologies. This conclusion is supported by the Fe_2O_3 content of Mozaan, at 25 wt%. The Makganyene diamictite also has high iron content (18.4 wt%) and comprises a ferruginous matrix containing Griqualand BIF clasts. Dwyka West has a higher iron content than its Palaeozoic counterparts, at 9.77 wt%, and BIF clasts were observed in the Dwyka West core sample (Fig. S5). Moreover, the most negative Si isotope compositions in the Neoproterozoic diamictites are from those that contain reworked BIF and, in places, ferruginous matrix (e.g. Numees, Kaigas).

The relatively heavy δ^{30}Si values for the Neoproterozoic Blaubeker diamictite and Palaeoproterozoic diamictites (Duitschland, Gowganda, Bottle Creek) also require explanation. One mechanism for generating relatively high δ^{30}Si is incorporation of silicified material into, or silicification of, the diamictites. As the δ^{30}Si of the modern ocean is ∼ +1.1‰ and Archaean seawater is inferred to reach up to ∼ +2‰ heavier (Stefurak et al., 2015), seawater silicification drives δ^{30}Si to positive values. Post-depositional silicification from hydrothermal fluids also imparts anomalous δ^{30}Si values, e.g. the −5.0‰ to +2.0‰ range reported for sinter deposits (Kleine et al., 2018). However, the only visibly silicified diamictite is Afrikander, with a δ^{30}Si value indistinguishable from Phanerozoic UCC and loess, suggesting silicification is not the source of the isotopically heavy δ^{30}Si values. Thus, whilst post-depositional siliceous hydrothermal fluids could have imparted heavy Si values to the Blaubeker and Palaeoproterozoic diamictites, a more straightforward explanation is that the constituent lithologies dominating these composite samples influenced their Si-isotopic compositions. For example, many (Blaubeker, Ramsay Lake, Bruce, Gowganda) if not all of these diamictites are dominated by granitoid and quartzite clasts, highlighting the likely influence of a SiO_2-rich source lithology-prone to having high δ^{30}Si relative to modern basalts and average UCC (Savage et al., 2012).

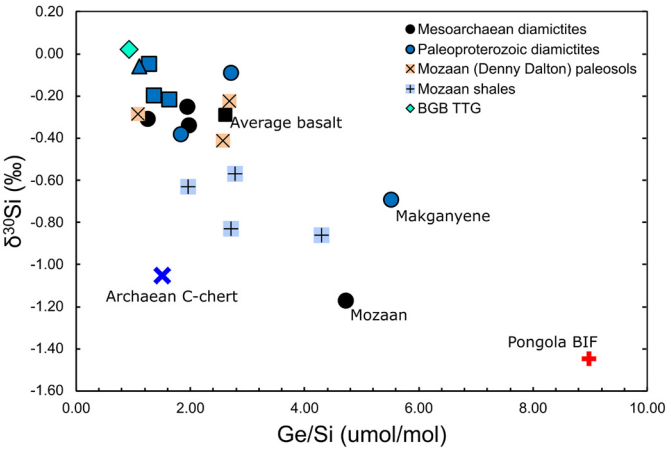

Fig. 3. Ge/Si versus δ^{30}Si of Archaean and Palaeoproterozoic diamictites with respect to coeval paleosols and shales from the Mozaan Group (data from Delvigne et al., 2016) as well as TTGs (data from André et al., 2022) from the Barberton Greenstone Belt (BGB, located on the Kaapvaal craton). BIF, basalt, and C-chert data are listed in Table S6 for Ge/Si polygon. Diamictite Ge data from Gaschnig et al. (2016). Higher Ge/Si reflects hydrothermally sourced Si, whereas lower Ge/Si likely reflects continental input of Si; hence BIF typically has higher Ge/Si ratios. This figure illustrates the influence of BIF in generating negative Si isotope signatures, specifically in the Mozaan and Makganyene diamictite composites.

5.3. Crustal inputs into diamictite source

There are several potential sources derived from lithologies with distinct Si isotope compositions that could explain variable diamictite δ^{30}Si values. Metrics such as Ge/Si help differentiate between possible endmember lithologies with similar Si isotope values and, when plotted against δ^{30}Si (e.g. Fig. 3), can be compared to the diamictites to elucidate their source rocks. Ge/Si ratios can highlight contribution of BIF to the diamictite source; Ge/Si distinguishes between hydrothermal and continental silicon (Delvigne et al., 2012), wherein higher Ge/Si is taken to reflect hydrothermally-sourced Si. Hence, BIF typically has higher Ge/Si ratios, and its influence is reflected in the diamictites with light Si isotope signatures compared to coeval rocks from the same craton, like TTGs and shales (Fig. 3).

To further understand the contribution of source materials to diamictite deposits- and therefore what lithologies were at the surface during glaciation- we model the mixing of isotopic reservoirs with potentially variable δ^{30}Si of the glacially-milled continental

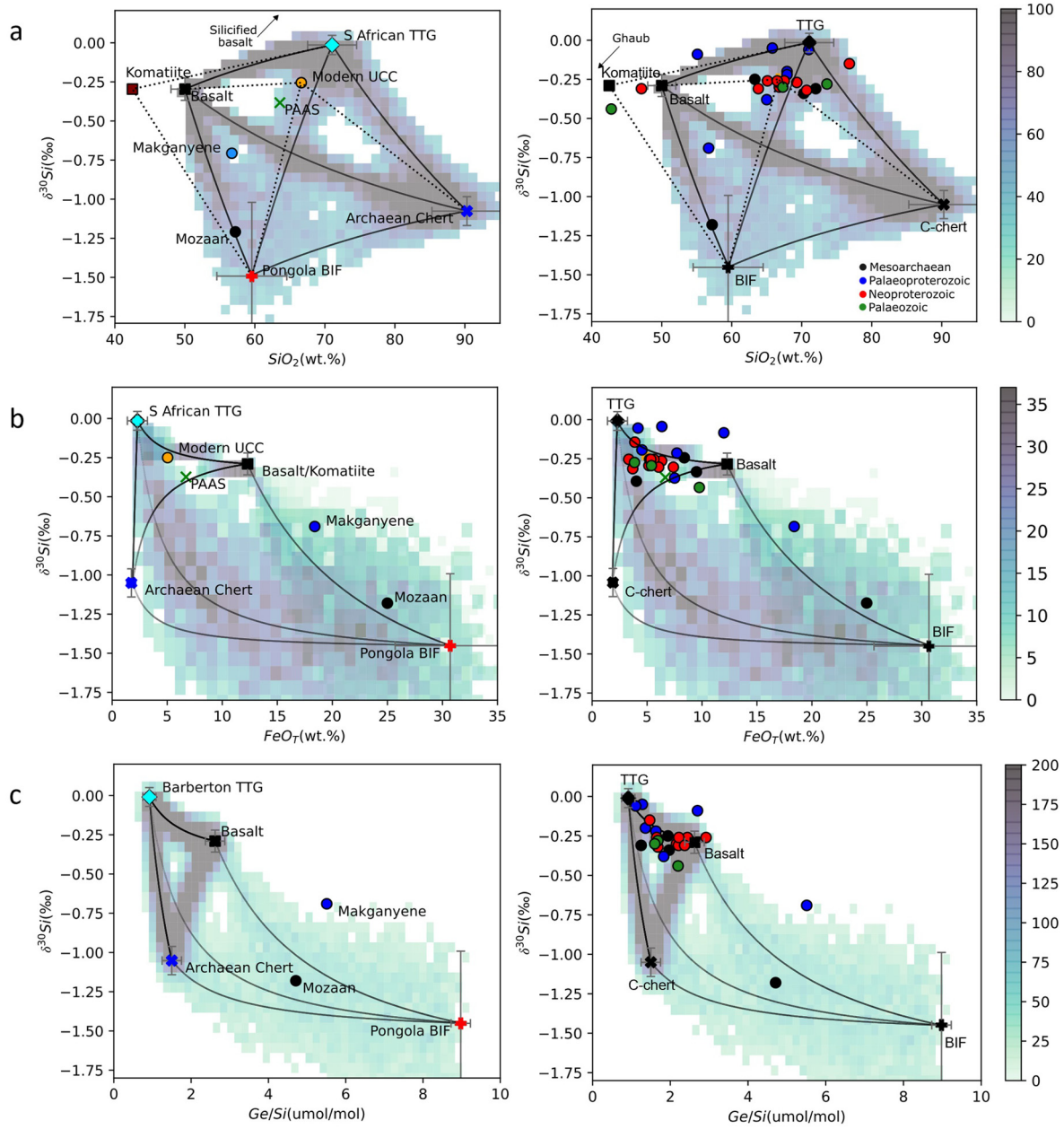

Fig. 4. δ^{30}Si-oxide mixing polygons with inferred diamictite source lithologies to explain anomalous sample values. Panels on the left side show only Mozaan and Makganyene diamictites (having the lowest δ^{30}Si values), whereas panels on the right show all diamictite data as coloured circles. Coloured heat maps represent Monte Carlo (MC) simulations of 10,000 iterations to propagate error associated with variable Si isotope literature data for each chosen endmember. Colour bars on right side denote frequency of data points in each kernel. Dark grey error bars are 2 s.d. on each endmember value. For detailed mixing curve inputs and sources see Table S6. For full MC description see Appendix A. a) δ^{30}Si-SiO_2 mixing polygon. b) FeO_T -SiO_2 mixing polygon, which highlights the influence of BIF in imparting the anomalous Si signatures. c) Ge/Si-SiO_2 mixing polygon to build on Fig. 3.

crust using silica, iron, and Ge/Si as end-member proxies. This modelling aims to clarify the source of anomalous diamictite Si isotope signatures by simulating the proportion of likely protolith lithologies required to impart such values and test our conclusions regarding the sources of Si isotope heterogeneity in the diamictite data. To encompass the complete range of possible δ^{30}Si values for different protoliths and propagate error associated with the data, we generated Monte Carlo (MC) simulations of 10,000 runs in Python (represented by coloured data maps in Fig. 4; input parameters given in Table S6). These MC simulations were designed to illustrate the maximum possible range of values in source materials that could contribute to the diamictite δ^{30}Si signatures, and endmembers were selected by averaging values from the literature for likely diamictite source material, such as BIF, chert, and basalt. These MC models (discussed in greater detail in Appendix A) show the relative abundance of endmembers by depicting the higher probability parts of the composition space, and they still define discrete fields in which our samples plot. Namely, the mixing polygons show the importance of certain lithologies and eliminate others.

As discussed above, the strikingly negative δ^{30}Si Mozaan and Makganyene diamictites derive their light Si isotope signatures from several possible sources. One endmember lithology that can impart very low δ^{30}Si values is Archaean C-chert, a siliceous precipitate formed from either seawater, hydrothermal fluids, or a mixture of both (Marin-Carbonne et al., 2014); however, the mixing model indicates that the silica content of Mozaan is too low for chert to be the likely source of its negative Si isotope value

(Fig. 4a). A clay-rich source (represented here by Post-Archaean Australian Shale, PAAS, and Mozaan shale) can also be ruled out (Fig. 4b) as its low iron content is insufficient to account for the composition of those two diamictites. By contrast, the FeO_T and Ge/Si mixing polygons (Figs. 4b and 4c) show the influence of BIF in generating highly negative diamictite δ^{30}Si values. In all models, highly negative diamictite data appear to be influenced by a mixture of a basaltic or komatiitic source and BIF and suggest that generating such values would require a high proportion of BIF in the diamictites, particularly the Mozaan composite. It is possible that the BIF component in the Mozaan source had a more extreme negative δ^{30}Si signature than is reported here, and its signal was muted by averaging with other lithologies with isotopically heavier Si; world-wide, BIF δ^{30}Si can be as low as $-4.29‰$ (Chakrabarti et al., 2012). Equally, the crust sampled during the Mesoarchaean glaciation that deposited the Mozaan diamictite may have been dominated by BIF, given the prevalence of iron formation in Archaean terranes (e.g. Farquhar et al., 2014). Regardless, it is feasible that iron-formation-rich material with light Si existed in the region scoured by glaciers, imparting low δ^{30}Si values to the South African diamictites. By contrast, the slightly isotopically heavy signatures in Palaeoproterozoic diamictites likely reflect the influence of a TTG-like source (Figs. 4a and 4b) due to their higher silica and lower iron content. From the mixing models, the oldest continental crust, as sampled by the South African diamictites, was likely dominated by different proportions of komatiite or basalt, BIF, and TTG, comprising an early heterogeneous UCC with respect to Si isotopes.

5.4. Temporal δ^{30}Si trends in the upper continental crust

5.4.1. Reduced δ^{30}Si heterogeneity through time: a Kaapvaal case study

The secular trend of silicon isotopes in the UCC becoming more homogeneous through time is particularly apparent for the nine diamictite composites deposited on the Kaapvaal craton; these diamictites track a local record of the UCC chemical composition from ~2.9–0.3 Ga and provide the opportunity to compare isotopic trends over time in material sourced from the same general region.

The wide variability in δ^{30}Si of Mesoarchaean diamictites is from the strongly negative Mozaan sample, whereas the other three diamictites in this age group (Afrikander, Promise, Coronation) approximate the modern UCC value. These three are members of the Witwatersrand Supergroup and are spatially distinct from the Mozaan sample, from the Pongola Supergroup. Notably, ^{182}W isotope analyses of the four Mesoarchaean diamictites reveal a negative correlation with the Si isotope data reported here; the Witwatersrand samples exhibit highly negative μ^{182}W values, whereas the Mozaan sample is not resolvably different from the W standard (Mundl et al., 2018). Negative μ^{182}W values are unusual in ancient continental crust, which more commonly has positive μ^{182}W values. Such negative values have been observed only in unusual komatiites from Schapenburg, South Africa, in the Barberton greenstone belt (Mundl et al., 2018). Thus, anomalous W signatures in the diamictites were interpreted by Mundl et al. (2018) to reflect significant contribution from Schapenburg-like komatiites or material with more negative μ^{182}W values. The possible komatiite signature from W isotopes and strong BIF signature inferred from Si isotopes document significant lithologic and isotopic heterogeneity in the Mesoarchaean Kaapvaal craton. Additionally, the fact that these samples are composites–mixtures of many individual diamictite units–and they still exhibit such strong affinities for specific lithologies implies that their isotopically distinct source rocks were either a dominant spatial component of the land surfaces scoured by glaciers, or the source rocks had more extreme isotopic values than other constituent lithologies. Regardless, the Archaean UCC, as recorded by Si and W isotopic signatures of South African diamictites, was heterogeneous.

The Palaeoproterozoic diamictites from South Africa (Duitschland, Timeball Hill, Makganyene) also show a large spread in δ^{30}Si, from one of the lowest values in the sample set to one of the highest, defining a slightly narrower range than the Archaean samples. Makganyene, which likely obtained its negative signature from BIF, is significantly heavier than the Archaean Mozaan sample, suggesting a reworking and homogenisation (i.e. erosion and re-sedimentation or recycling of the constituent lithologies during multiple weathering cycles) of the Kaapvaal crust between the Mesoarchaean and Palaeoproterozoic. The Timeball Hill diamictite has slightly negative δ^{30}Si, at the lower bounds of the error on that of modern UCC. The Palaeozoic Dwyka West and Dwyka East samples define the smallest δ^{30}Si range, with the latter being indistinguishable from the modern UCC. The Dwyka West sample is slightly more negative than the modern UCC error and is more iron-rich than the contemporaneous Dwyka East diamictite, pointing to the continuing influence of BIF in its provenance. The δ^{30}Si in this sample much more closely approximates modern UCC δ^{30}Si relative to that of the Mozaan and Makganyene diamictites, strengthening the argument for homogenising Si isotopes in the crust over time.

5.4.2. Disappearance of TTG and BIF

The shift toward modern Si isotope signatures after the Palaeoproterozoic (Fig. 5) may be linked to the decreased proportion of TTG suites as major constituents of continental crust. While TTGs dominate ancient terranes, they were only minor components of juvenile crust by end of the Archaean and were superseded by potassic I-type granitoids, reflecting a fundamental shift in the generation of continental crust (e.g. Laurent et al., 2014). The decreased importance of TTG is reflected in the Si isotope composition of the upper continental crust during this tectonic transition. TTG δ^{30}Si values were recently found to be, on average, heavier than Phanerozoic granitic analogues; whereas modern granites exhibit values around $-0.23 \pm 0.15‰$ (2 s.d., Savage et al., 2012), Archaean TTGs from the Kaapvaal craton have an average δ^{30}Si of $\sim +0.01‰$ (André et al., 2019), and this result is supported by similarly heavy Si isotope compositions reported for other global TTGs (Deng et al., 2019). We attribute heavy Si isotope values of the TTG-clast bearing Palaeoproterozoic diamictites to being sourced from TTG, which have resolvably heavier δ^{30}Si values compared to the BSE (Fig. 5a). Subsequent contraction of δ^{30}Si values in the UCC towards Phanerozoic-granite-like signatures likely reflects the increasing scarcity of exposed TTG suites after the Archaean.

Like TTGs, banded iron formations were a more dominant component in ancient continental crust relative to the younger rock record, with their disappearance at c. ~1.88 Ga being tied to fundamental shifts in the atmosphere and ocean redox state as a result of planetary oxygenation (e.g. Farquhar et al., 2014). This disappearance may be recorded by the reduced magnitude of negative diamictite δ^{30}Si values over time. The cessation of Superior-type BIF around ~1.88 Ga does not coincide with the inferred timing of planetary oxygenation, necessitating a more complex geochemical mechanism for their disappearance, one that is inferred to reflect to a change in oceanic redox state or deep mantle processes (e.g. Farquhar et al., 2014 and references therein). The reduction in the magnitude of negative δ^{30}Si in diamictite composites through time, evident in the Kaapvaal samples, might record this disappearance of iron formations and subsequent recycling and homogenising of BIF-rich material to a heavier average δ^{30}Si UCC value. The rise in atmospheric oxygen and consequent geochemical changes associated with the scarcity of BIF seemingly coincide with an initial narrowing of Si isotope values in the Palaeoproterozoic (Fig. 5a),

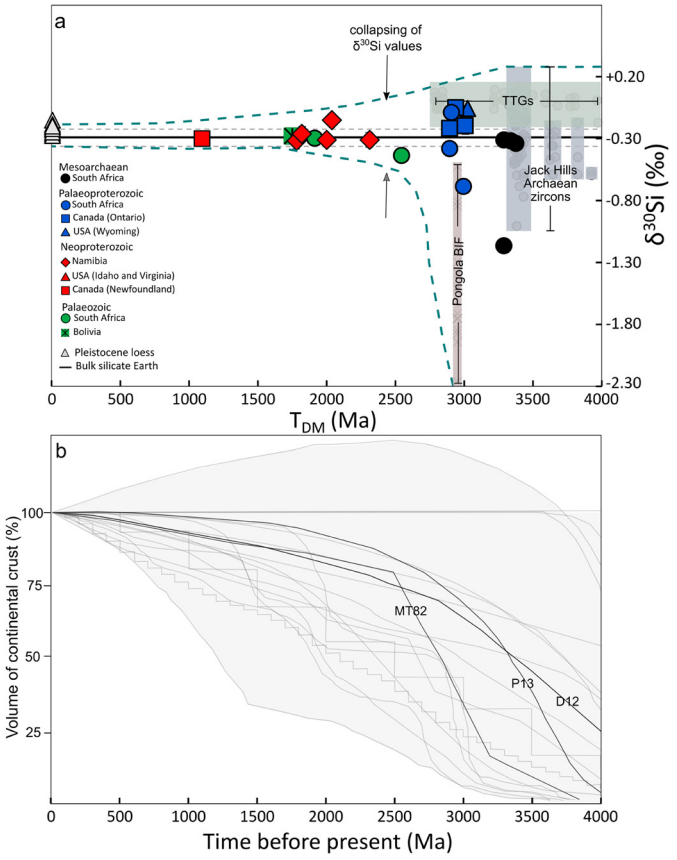

Fig. 5. Plot of diamictite δ^{30}Si against T_{DM} Nd model ages (from Gaschnig et al., 2022). Error bars are 95% s.e. Solid black line is $\delta^{30}Si_{BSE}$ of -0.29 ± 0.07‰ (Savage et al., 2014) and the dashed lines represent 2s.d. error. Teal dashed lines encompass range of δ^{30}Si through time. Pleistocene loess data from Savage et al. (2013b); TTG data from André et al. (2019) and Deng et al. (2019); Pongola BIF data from Delvigne et al. (2012); Jack Hills zircon data from Trail et al. (2018). Continental growth curves in light grey, from various published models (normalised to the present volume of crust) after Korenaga (2018) highlighting those of McLennan and Taylor (1982) (MT82), Pujol et al. (2013) (P13), and Dhuime et al. (2012) (D12).

and the eventual disappearance of BIF around ~1.9 Ga aligns with the reduction of anomalously negative δ^{30}Si values apparent in the younger samples.

5.5. Implications for crustal stabilisation

The homogenisation of silicon isotopes in the crust recorded by δ^{30}Si values of ancient glacial diamictites implies a secular change in geodynamic regime throughout Earth history. Diamictite Si isotope signatures appear to contract to a narrow range shortly after ~2.5 Ga (Fig. 5a), a time by which some authors suggest Earth's global tectonic regime had shifted to a style dominated by subduction-driven plate tectonics (e.g. McLennan and Taylor, 1982; Pujol et al., 2013). However, there is an offset from when this inflection is recorded in the Si isotope data because by their nature, diamictites consist of material that is older than their deposition age. While many workers purport that this tectonic shift occurred in the late Archaean (see Hawkesworth et al., 2020 and references therein), homogenisation of diamictite Si isotopes appears to happen later; Palaeoproterozoic diamictites exhibit a narrower range than the oldest samples, with the modern UCC δ^{30}Si signature reached by the Neoproterozoic. Notably, the ~2.4-2.3 Ga diamictites consist of material that is Archaean in age, according to their Nd model ages (Gaschnig et al., 2022), and when plotted against δ^{30}Si (Fig. 5a) show better alignment between homogenisation of Si with the inferred global onset of subduction. This cross-plot shows that δ^{30}Si values appear to narrow to the modern UCC value somewhere between 2.5 and 3.0 Ga. Moreover, the diamictite samples with variable δ^{30}Si signatures all have Archaean Nd model ages (e.g. the extremely light Makganyene, and the heavy Gowganda, Wyoming, and Duitschland diamictites, have Archaean model ages, as does the slightly light Palaeozoic Dwyka West diamictite).

The diamictite model ages could be explained by the initially wide-ranging Si isotope values in the earliest crust becoming homogenised as this crust was reworked and subsequently scoured by glaciers – as cratonisation processes stabilised emergent crust. Silicon isotopes of Jack Hills Hadean zircons support this, as they span a wide δ^{30}Si range (Trail et al., 2018; Fig. 5a), further illustrating silicon isotope heterogeneity in the oldest preserved fragments of crust. Crustal reworking homogenised this isotopic heterogeneity as crustal growth rates declined and stabilisation of the continental lithosphere was able to support subduction. The timing of craton stabilisation is highlighted by continental growth curves in Fig. 5b (after Korenaga, 2018 and references therein). Although the rate of crustal growth is highly debated, these curves are based on extensive worldwide databases, instilling confidence in the crustal reworking trend and plate tectonic onset inferred from such proxies. However, the curves incorporate major assumptions; drawbacks of using combined Hf and O isotopes in zircons (e.g. Dhuime et al., 2012) include the assumption that O-isotope-filtered zircons, thought to have mantle compositions, will produce Hf model ages indicative of crust formation (Payne et al., 2016). Moreover, both Hf and Nd model ages rely on assumed parameters for a depleted mantle source differing between authors, resulting in model age calculations that can be significantly different (Chauvel et al., 2014). Nevertheless, several geochemical and geologic approaches have independently converged on a conclusion that ~65% of the present continental crust volume was formed by ~3.0 Ga, at which point the lithosphere became strong enough to support crustal thickening and reworking (Hawkesworth et al., 2019).

The Si isotope data presented here support this view of late Archaean cratonisation and subsequent reworking. Critically, Si isotopes are potentially more robust than previous elemental proxies used to construct continental growth curves as they are not predicated on assumptions about present and past volumes of continental crust necessary to create these models of craton stabilisation. In the plot of δ^{30}Si against Nd model ages (Fig. 5a), the narrowing of diamictite Si isotope signatures aligns with many continental growth studies, thus, secular homogenisation of δ^{30}Si values in glacial diamictites supports the late Archaean cratonisation model by recording a history of the primary processes in the ancient continental crust independent of zircon and fine-grained sediment databases. The silicon isotope data for glacial diamictites record a history of lithologically distinct cratons whose Si isotopes were influenced by BIF and TTG in the Archaean, followed by stabilisation of the lithosphere resulting in crustal reworking that effectively homogenised Si isotopes in the continental crust after ~3.0 Ga.

6. Conclusions

1. The large range in δ^{30}Si of ~2.9-2.3 Ga glacial diamictites compared to the narrower range observed in younger diamictites and Phanerozoic loess suggests greater Si isotope heterogeneity in the early continental crust that became progressively homogenised over geological time.
2. The similarity of negative δ^{30}Si values in BIF with those of the Mozaan and Makganyene diamictite composites, together with their high Fe content and low Al content, reflects the influence of iron formations in diamictite provenances. The disappearance of BIF from the rock record from the chemical evolution

of Earth's atmosphere is recorded in the disappearance of isotopically light diamictite composites. By contrast, isotopically heavy Si in some Palaeoproterozoic diamictites reflects TTG in their provenance.

3. South African diamictite Si isotope trends demonstrate progressive homogenisation of the crust despite the influence of local provenance, as the δ^{30}Si values of Kaapvaal samples approach the modern upper continental crust Si isotope signature over time. The light δ^{30}Si of Makganyene and somewhat negative δ^{30}Si of the Dwyka West diamictite, combined with their Archaean Nd model ages, illustrate the reworking of crust over time to homogenise Si isotope signatures in the UCC.
4. The Si isotope data reported here for ancient glacial diamictites support the view that much of Earth's continental crust was generated and formed stable cratons by the late Archaean, followed by the onset of subduction-driven plate tectonics. The homogenisation of initially heterogeneous Si isotope values in the UCC through time reflects the post-Archaean reworking of ancient, lithologically disparate cratons and further advances the continental growth argument using this robust isotope system.

CRediT authorship contribution statement

All authors contributed to the conceptualisation and formulation of ideas as the work progressed. All authors contributed to writing–review & editing. MM conducted formal analysis and wrote the original draft. RR and RG provided samples. PS, RR, and RG secured funding that contributed to the final report. Madeleine Murphy: Formal analysis, Writing–Original Draft.
Paul Savage: Conceptualisation, Funding acquisition, Writing–Review & Editing.
Nicholas Gardiner: Conceptualisation, Writing–Review & Editing.
Anthony Prave: Conceptualisation, Writing–Review & Editing.
Richard Gaschnig: Resources, Writing–Review & Editing.
Roberta Rudnick: Conceptualisation, Funding acquisition, Writing–Review & Editing.

Declaration of competing interest

The authors declare that they have no known competing financial interests or personal relationships that could have appeared to influence the work reported in this paper.

Acknowledgements

We thank Robert Steele and Hana Jurikova for their stellar analytical support in the STAiG labs, as well as Eva Stueeken for the use of their furnace facilities at St Andrews. We would like to thank Luc André and one anonymous reviewer for insightful input that greatly improved the manuscript, as well as Laurence Coogan for his thoughtful editorial handling and comments. This work was supported by PhD funding to MM by the University of St Andrews School of Earth and Environmental Sciences and the Handsel scheme, as well as by NERC grant NE/R002134/1 to PS and NSF grant EAR-1321954 to RR and RG.

Appendix. Supplementary material

Supplementary material related to this article can be found online at https://doi.org/10.1016/j.epsl.2022.117620.

References

André, L., Abraham, K., Hofmann, A., Monin, L., Kleinhanns, I.C., Foley, S., 2019. Early continental crust generated by reworking of basalts variably silicified by seawater. Nat. Geosci. 12 (9), 769–773. https://doi.org/10.1038/s41561-019-0408-5.

André, L., Monin, L., Hofmann, A., 2022. The origin of early continental crust: new clues from coupling Ge/Si ratios with silicon isotopes. Earth Planet. Sci. Lett. 582, 117415. https://doi.org/10.1016/j.epsl.2022.117415.

Brown, M., Johnson, T., Gardiner, N.J., 2020. Plate tectonics and the Archean Earth. https://doi.org/10.1146/annurev-earth-081619.

Canfield, D.E., 2014. Proterozoic Atmospheric Oxygen, second edition. Treatise on Geochemistry, vol. 6, pp. 197–216.

Chakrabarti, R., Knoll, A.H., Jacobsen, S.B., Fischer, W.W., 2012. Si isotope variability in Proterozoic cherts. Geochim. Cosmochim. Acta 91, 187–201. https://doi.org/10.1016/J.GCA.2012.05.025.

Chauvel, C., Garçon, M., Bureau, S., Besnault, A., Jahn, B., Ding, Z., 2014. Constraints from loess on the Hf–Nd isotopic composition of the upper continental crust. Earth Planet. Sci. Lett. 388, 48–58. https://doi.org/10.1016/J.EPSL.2013.11.045.

Chen, K., Rudnick, R.L., Wang, Z., Tang, M., Gaschnig, R.M., Zou, Z., He, T., Hu, Z., Liu, Y., 2020. How mafic was the Archean upper continental crust? Insights from Cu and Ag in ancient glacial diamictites. Geochim. Cosmochim. Acta 278, 16–29. https://doi.org/10.1016/J.GCA.2019.08.002.

Chen, K., Walker, R.J., Rudnick, R.L., Gao, S., Gaschnig, R.M., Puchtel, I.S., Tang, M., Hu, Z.C., 2016. Platinum-group element abundances and Re–Os isotopic systematics of the upper continental crust through time: evidence from glacial diamictites. Geochim. Cosmochim. Acta 191, 1–16. https://doi.org/10.1016/J.GCA.2016.07.004.

De La Rocha, C.L., Brzezinski, M.A., Deniro, M.J., 2000. A first look at the distribution of the stable isotopes of silicon in natural waters. Geochim. Cosmochim. Acta 64 (14), 2467–2477. https://doi.org/10.1016/S0016-7037(00)00373-2.

Delstanche, S., Opfergelt, S., Cardinal, D., Elsass, F., André, L., Delvaux, B., 2009. Silicon isotopic fractionation during adsorption of aqueous monosilicic acid onto iron oxide. Geochim. Cosmochim. Acta 73 (4), 923–934. https://doi.org/10.1016/J.GCA.2008.11.014.

Delvigne, C., Cardinal, D., Hofmann, A., André, L., 2012. Stratigraphic changes of Ge/Si, REE+Y and silicon isotopes as insights into the deposition of a Mesoarchaean banded iron formation. Earth Planet. Sci. Lett. 355–356, 109–118. https://doi.org/10.1016/J.EPSL.2012.07.035.

Delvigne, C., Opfergelt, S., Cardinal, D., Hofmann, A., André, L., 2016. Desilication in Archean weathering processes traced by silicon isotopes and Ge/Si ratios. Chem. Geol. 420, 139–147. https://doi.org/10.1016/j.chemgeo.2015.11.007.

Deng, Z., Chaussidon, M., Guitreau, M., Puchtel, I.S., Dauphas, N., Moynier, F., 2019. An oceanic subduction origin for Archaean granitoids revealed by silicon isotopes. Nat. Geosci. 12 (9), 774–778. https://doi.org/10.1038/s41561-019-0407-6.

Dhuime, B., Hawkesworth, C.J., Cawood, P.A., Storey, C.D., 2012. A change in the geodynamics of continental growth 3 billion years ago. Science 335 (6074), 1334–1336. https://doi.org/10.1126/SCIENCE.1216066.

Farquhar, J., Zerkle, A.L., Bekker, A., 2014. Geologic and Geochemical Constraints on Earth's Early Atmosphere, second edition. Treatise on Geochemistry, vol. 6, pp. 91–138.

Furnes, H., Dilek, Y., De Wit, M., 2015. Precambrian greenstone sequences represent different ophiolite types. Gondwana Res. 27 (2), 649–685. https://doi.org/10.1016/J.GR.2013.06.004.

Gaschnig, R.M., Horan, M.F., Rudnick, R.L., Vervoort, J.D., Fisher, C.M., 2022. History of crustal growth in Africa and the Americas from detrital zircon and Nd isotopes in glacial diamictites. Precambrian Res. 373, 106641. https://doi.org/10.1016/j.precamres.2022.106641.

Gaschnig, R.M., Rudnick, R.L., McDonough, W.F., Kaufman, A.J., Hu, Z., Gao, S., 2014. Onset of oxidative weathering of continents recorded in the geochemistry of ancient glacial diamictites. Earth Planet. Sci. Lett. 408, 87–99. https://doi.org/10.1016/J.EPSL.2014.10.002.

Gaschnig, R.M., Rudnick, R.L., McDonough, W.F., Kaufman, A.J., Valley, J.W., Hu, Z., Gao, S., Beck, M.L., 2016. Compositional evolution of the upper continental crust through time, as constrained by ancient glacial diamictites. Geochim. Cosmochim. Acta 186, 316–343. https://doi.org/10.1016/J.GCA.2016.03.020.

Georg, R.B., Reynolds, B.C., Frank, M., Halliday, A.N., 2006. New sample preparation techniques for the determination of Si isotopic compositions using MC-ICPMS. Chem. Geol. 235 (1–2), 95–104. https://doi.org/10.1016/J.CHEMGEO.2006.06.006.

Georg, R.B., Zhu, C., Reynolds, B.C., Halliday, A.N., 2009. Stable silicon isotopes of groundwater, feldspars, and clay coatings in the Navajo Sandstone aquifer, Black Mesa, Arizona, USA. Geochim. Cosmochim. Acta 73 (8), 2229–2241. https://doi.org/10.1016/J.GCA.2009.02.005.

Greaney, A.T., Rudnick, R.L., Romaniello, S.J., Johnson, A.C., Gaschnig, R.M., Anbar, A.D., 2020. Molybdenum isotope fractionation in glacial diamictites tracks the onset of oxidative weathering of the continental crust. Earth Planet. Sci. Lett. 534, 116083. https://doi.org/10.1016/J.EPSL.2020.116083.

Halliday, A.N., 2014. The origin and earliest history of the Earth. In: Davis, A.M. (Ed.), Planets, Asteroids, Comets and the Solar System, vol. 2, pp. 149–211.

Hatton, J.E., Hendry, K.R., Hawkings, J.R., Wadham, J.L., Benning, L.G., Blukis, R., Roddatis, V., Ng, H.C., Wang, T., 2021. Physical weathering by glaciers enhances silicon mobilisation and isotopic fractionation. Geochem. Perspect. Lett., 7–12. https://doi.org/10.7185/GEOCHEMLET.2126.

Hatton, J.E., Hendry, K.R., Hawkings, J.R., Wadham, J.L., Opfergelt, S., Kohler, T.J., Yde, J.C., Stibal, M., Žárský, J.D., 2019. Silicon isotopes in Arctic and sub-Arctic glacial meltwaters: the role of subglacial weathering in the silicon cycle. Proc. R. Soc. A 475 (2228). https://doi.org/10.1098/RSPA.2019.0098.

Hawkesworth, C.J., Cawood, P.A., Dhuime, B., 2019. Rates of generation and growth of the continental crust. Geosci. Front. 10 (1), 165–173. https://doi.org/10.1016/J.GSF.2018.02.004.

Hawkesworth, C.J., Cawood, P.A., Dhuime, B., 2020. The evolution of the continental crust and the onset of plate tectonics. Front. Earth Sci., 326. https://doi.org/10.3389/FEART.2020.00326.

Jacobsen, S.B., Ranen, M.C., Petaev, M.I., Remo, J.L., O'Connell, R.J., Sasselov, D.D., 2008. Isotopes as clues to the origin and earliest differentiation history of the Earth. Philos. Trans. - Royal Soc., Math. Phys. Eng. Sci. 366 (1883), 4129–4162. https://doi.org/10.1098/rsta.2008.0174.

Kleine, B.I., Stefánsson, A., Halldórsson, S.A., Whitehouse, M.J., Jónasson, K., 2018. Silicon and oxygen isotopes unravel quartz formation processes in the Icelandic crust. Geochem. Perspect. Lett. 7, 5–11. https://doi.org/10.7185/GEOCHEMLET.1811.

Korenaga, J., 2018. Crustal evolution and mantle dynamics through Earth history. Philos. Trans. - Royal Soc., Math. Phys. Eng. Sci. 376 (2132), 20170408. https://doi.org/10.1098/rsta.2017.0408.

Laurent, O., Martin, H., Moyen, J.F., Doucelance, R., 2014. The diversity and evolution of late-Archean granitoids: evidence for the onset of "modern-style" plate tectonics between 3.0 and 2.5 Ga. Lithos 205, 208–235. https://doi.org/10.1016/j.lithos.2014.06.012.

Lee, C.-T.A., Yeung, L.Y., McKenzie, N.R., Yokoyama, Y., Ozaki, K., Lenardic, A., 2016. Two-step rise of atmospheric oxygen linked to the growth of continents. Nat. Geosci. 9 (6), 417–424. https://doi.org/10.1038/ngeo2707.

Li, S., Gaschnig, R.M., Rudnick, R.L., 2016. Insights into chemical weathering of the upper continental crust from the geochemistry of ancient glacial diamictites. Geochim. Cosmochim. Acta 176, 96–117. https://doi.org/10.1016/J.GCA.2015.12.012.

Marin-Carbonne, J., Robert, F., Chaussidon, M., 2014. The silicon and oxygen isotope compositions of Precambrian cherts: a record of oceanic paleo-temperatures? Precambrian Res. 247, 223–234. https://doi.org/10.1016/J.PRECAMRES.2014.03.016.

McLennan, S.M., Taylor, S.R., 1982. Geochemical constraints on the growth of the continental crust. J. Geol. 90 (4), 347–361. https://doi.org/10.1086/628690.

Mundl, A., Walker, R.J., Reimink, J.R., Rudnick, R.L., Gaschnig, R.M., 2018. Tungsten-182 in the upper continental crust: evidence from glacial diamictites. Chem. Geol. 494, 144–152. https://doi.org/10.1016/J.CHEMGEO.2018.07.036.

Opfergelt, S., Georg, R.B., Delvaux, B., Cabidoche, Y.M., Burton, K.W., Halliday, A.N., 2012. Silicon isotopes and the tracing of desilication in volcanic soil weathering sequences, Guadeloupe. Chem. Geol. 326–327, 113–122. https://doi.org/10.1016/J.CHEMGEO.2012.07.032.

Payne, J.L., McInerney, D.J., Barovich, K.M., Kirkland, C.L., Pearson, N.J., Hand, M., 2016. Strengths and limitations of zircon Lu-Hf and O isotopes in modelling crustal growth. Lithos 248–251, 175–192. https://doi.org/10.1016/J.LITHOS.2015.12.015.

Poitrasson, F., 2017. In: Teng, F.-Z., Watkins, J., Dauphas, N. (Eds.), 8 Silicon Isotope Geochemistry. De Gruyter, pp. 289–344.

Pujol, M., Marty, B., Burgess, R., Turner, G., Philippot, P., 2013. Argon isotopic composition of Archaean atmosphere probes early Earth geodynamics. Nature 498 (7452), 87–90. https://doi.org/10.1038/nature12152.

Rudnick, R.L., Gao, S., 2014. Composition of the continental crust. In: Treatise on Geochemistry, pp. 1–51.

Savage, P.S., Armytage, R.M.G., Georg, R.B., Halliday, A.N., 2014. High temperature silicon isotope geochemistry. Lithos 190–191, 500–519. https://doi.org/10.1016/J.LITHOS.2014.01.003.

Savage, P.S., Georg, R.B., Williams, H.M., Halliday, A.N., 2013a. Silicon isotopes in granulite xenoliths: insights into isotopic fractionation during igneous processes and the composition of the deep continental crust. Earth Planet. Sci. Lett. 365, 221–231. https://doi.org/10.1016/J.EPSL.2013.01.019.

Savage, P.S., Georg, R.B., Williams, H.M., Halliday, A.N., 2013b. The silicon isotope composition of the upper continental crust. Geochim. Cosmochim. Acta 109, 384–399. https://doi.org/10.1016/J.GCA.2013.02.004.

Savage, P.S., Georg, R.B., Williams, H.M., Turner, S., Halliday, A.N., Chappell, B.W., 2012. The silicon isotope composition of granites. Geochim. Cosmochim. Acta 92, 184–202. https://doi.org/10.1016/J.GCA.2012.06.017.

Savage, P.S., Moynier, F., 2013. Silicon isotopic variation in enstatite meteorites: clues to their origin and Earth-forming material. Earth Planet. Sci. Lett. 361, 487–496. https://doi.org/10.1016/J.EPSL.2012.11.016.

Stefurak, E.J.T., Fischer, W.W., Lowe, D.R., 2015. Texture-specific Si isotope variations in Barberton Greenstone Belt cherts record low temperature fractionations in early Archean seawater. Geochim. Cosmochim. Acta 150, 26–52. https://doi.org/10.1016/j.gca.2014.11.014.

Tang, M., Chen, K., Rudnick, R.L., 2016. Archean upper crust transition from mafic to felsic marks the onset of plate tectonics. Science 351 (6271), 372–375. https://doi.org/10.1126/SCIENCE.AAD5513.

Trail, D., Boehnke, P., Savage, P.S., Liu, M.-C., Miller, M.L., Bindeman, I., 2018. Origin and significance of Si and O isotope heterogeneities in Phanerozoic, Archean, and Hadean zircon. Proc. Natl. Acad. Sci. 115 (41), 10287–10292. https://doi.org/10.1073/PNAS.1808335115.

Wang, B., Li, W.-Y., Deng, G., Huang, F., Yu, H.-M., Wang, B., Li, W.-Y., Deng, G., Huang, F., Yu, H.-M., 2019. Silicon isotope compositions of metaperidotites from the Franciscan Complex of California- implications for Si isotope fractionation during subduction dehydration. Lithos 350, 105228. https://doi.org/10.1016/J.LITHOS.2019.105228.

Wang, S.-J., Rudnick, R.L., Gaschnig, R.M., Wang, H., Wasylenki, L.E., 2019. Methanogenesis sustained by sulfide weathering during the Great Oxidation Event. Nat. Geosci. 12 (4), 296–300. https://doi.org/10.1038/s41561-019-0320-z.

Ziegler, K., Chadwick, O.A., White, A.F., Brzezinski, M.A., 2005. δ^{30}Si systematics in a granitic saprolite, Puerto Rico. Geology 33 (10), 817–820. https://doi.org/10.1130/G21707.1.